Modeling the Percutaneous Absorption of Solvent-Deposited Solids Over a Wide Dose Range

Fang Yu[a], Kevin Tonnis[a], Lijing Xu[b],
Joanna Jaworska[c] and Gerald B. Kasting[b*]

[a]College of Engineering and Applied Science
The University of Cincinnati

[b]The James L. Winkle College of Pharmacy
The University of Cincinnati

[c]The Procter & Gamble Company
Data and Modeling Sciences
Brussels Innovation Center, Belgium

[*]Correspondence:

Gerald B. Kasting
The James L. Winkle College of Pharmacy
University of Cincinnati Academic Health Center
Cincinnati, OH 45247-0514
Phone: 01 513-558-1817
Email: Gerald.Kasting@uc.edu

ABSTRACT:

The transient absorption of two skin care agents, niacinamide (nicotinamide, NA) and methyl nicotinate (MN), solvent-deposited on ex vivo human skin mounted in Franz diffusion cells has been analyzed according to a new variation on a recently published mechanistic skin permeability model (Yu et al. 2020. J Pharm Sci 110:2149-56). The model follows the absorption and evaporation of two components, solute and solvent, and it includes both a follicular transport component and a dissolution rate limitation for high melting, hydrophilic solids deposited on the skin. Explicit algorithms for improving the simulation of transient diffusion of solvent-deposited solids are introduced. The simulations can account for the ex vivo skin permeation time course of both NA and MN over a dose range exceeding 4.5 orders of magnitude. The model allows one to describe on a mechanistic basis why the percutaneous absorption rate of NA is approximately 60-fold lower than that of its lower melting, more lipophilic analog, MN. It furthermore suggests that MN perturbs stratum corneum barrier lipids and increases their permeability while NA does not, presenting a challenge to molecular modelers engaged in simulating biological lipid barriers.

Keywords: absorption; biophysical models; disposition; mathematical model; passive diffusion/transport; transdermal; pathways; percutaneous; permeability; skin

Introduction

Percutaneous absorption has historically drawn the attention of a wide range of scientists involved in skin care, topical and transdermal drug delivery and human safety groups within both government and industry. A broad experimental database exists, as well as many associated efforts to interpret these data on either a semiempirical or mechanistic basis. A useful review of the modeling field ca. 2011 was provided by Mitragotri et al.[1] Predictive models are highly desired in order to guide product development involving new active agents or compositions and to facilitate risk assessment of dermal exposures to chemicals in consumer or workplace exposures. Many, if not most, of these scenarios involve finite dose exposures.[2]

Our group has been involved in the development of transient diffusion models for dermal absorption for some time. Most recently we have incorporated a polar pathway for hydrophilic permeants into the model and moved it to a process engineering platform, gPROMS®.[3,4] In the present analysis we extend the model to accurately simulate a solvent deposition process in which a solid precipitate may form on the skin surface as the solvent evaporates. The disposition of both components is tracked. The balance between specific dose of solute and its solubility in the stratum corneum (SC) is a key element of the analysis, as are the crystallinity of the deposited solid and the details of the solvent dry down process on the skin surface and in the upper regions of hair follicles. We introduce specific elements to limit accumulation of solute in the hair follicle, accurately estimate time lags for follicular diffusion and control the dissolution rate of solvent-deposited solids. The developed algorithm is exemplified by an analysis of the transient permeation of niacinamide (nicotinamide, NA) and methyl nicotinate (MN) following solvent deposition onto excised human skin mounted in Franz diffusion cells.[5]

NA is a skin care ingredient providing both skin lightening and anti-ageing benefits.[6,7] MN is a rubefacient long used by dermatologists to assess skin barrier function in their patients by measuring time to redness or flushing.[8,9] Despite their moderate differences in octanol/water partition coefficient (K_{ow}) and molecular weight (MW) the two compounds show striking differences in both steady-state skin permeability and skin penetration from a finite dose, with MN >> NA in both cases. Ref. 5 discusses this behavior in terms of the physical properties of the permeants. Here we present a diffusion model designed to interpret the results on a mechanistic basis.

We note that the subject of solvent-deposited solids was explicitly treated by Anissimov and Roberts[10] using an elegant Laplace transform-based approach. They successfully analyzed finite dose dermal absorption data from Scheuplein and Ross[11] and also Crutcher and Maibach[12] using a model which included mass transfer resistances at the vehicle/SC and SC/receptor solution interfaces. These resistances can be interpreted as dissolution limitations and viable epidermis (VE) resistance, respectively. The examples presented – corticosterone, testosterone and testosterone proprionate – employed a VE resistance but did not require dissolution limitations. We present a counter example requiring a dissolution limitation (NA) and a hypothesis regarding how to anticipate this phenomenon, using a concept we term "hard" and "soft" solids. We refer the reader to Anissimov and Roberts[10] for an excellent review of finite dose diffusion experiments and analyses prior to 2001.

Mathematical Model

The dermal absorption model employed builds on a simpler model recently developed by our group to simulate the skin permeability of hydrophobic and hydrophilic chemicals[4] and called therein Model 2. Model 2 is a one-dimensional, transient diffusion/evaporation code built on the

gPROMS platform incorporating a vehicle layer, three skin layers and a follicular diffusion pathway. Its steady state properties have been thoroughly explored.[3,4] In this section we describe elaborations on Model 2 designed to yield more accurate simulations of transient diffusion associated with solvent-deposited solids. The revised model (Model 3) has the following new features: (1) a depth-dependent time lag, T_{lag}, in outer root sheath (ORS) flux is implemented to reduce the burst effect resulting from the mass transfer coefficient treatment of ORS permeability; (2) the surface roughness of the SC, δ_{sc}, is considered for limiting accumulation of solute in the infundibulum as the solvent film dries down. After vehicle thickness falls below δ_{sc}, solute transport from vehicle to infundibulum is blocked and the solution within the infundibulum is assumed to be well mixed. (3) A dissolution limitation expressed as an interfacial mass transfer coefficient, κ_{lip}, is applied for solid solute partitioning from the skin surface into the SC. This coefficient includes a thermodynamic term correcting partitioning of solutes having high solubilities or those which self-associate in aqueous solution.

We note that Models 2 and 3 are two-component diffusion/evaporation models that explicitly represent mass transport of both a solute and a solvent. The equations that follow are written in terms of the solute, which is usually the component of interest for topical or transdermal delivery. However, similar relationships apply for the solvent. The solvent-related equations are necessary to describe the dry down process and are also of interest in estimating its impact on skin permeability.

Time Lag for Follicular Diffusion

The geometry of the hair follicle embedded in the skin is that of Model 2, cf. Fig. 1 of Yu et al. 2020.[4] A closeup view of the ORS region is shown in Fig. 1. The follicular pathway is represented as an array of cylindrical prisms piercing all three layers of the skin. The infundibulum

is an annular space surrounded by the ORS epithelium. The ORS has a fixed total thickness (h_{ors}), which is comprised of an SC-like region (l_{scl}) and an ED-like region (l_{edl}). These thicknesses vary linearly with depth (z), representing decreasing keratinization with increasing depth.[13,14] They are described by Eqs. 1 and 2:

$$h_{ors} = l_{scl} + l_{edl} \tag{1}$$

$$\begin{cases} l_{scl} = h_{ors} \; and \; l_{edl} = 0 & 0 \le z \le h_{sc} \\ l_{scl} = h_{ors} \frac{L_1 - z}{L_1 - h_{sc}} \; and \; l_{edl} = h_{ors} \frac{z - h_{sc}}{L_1 - h_{sc}} & h_{sc} < z \le L_1 \end{cases} \tag{2a,b}$$

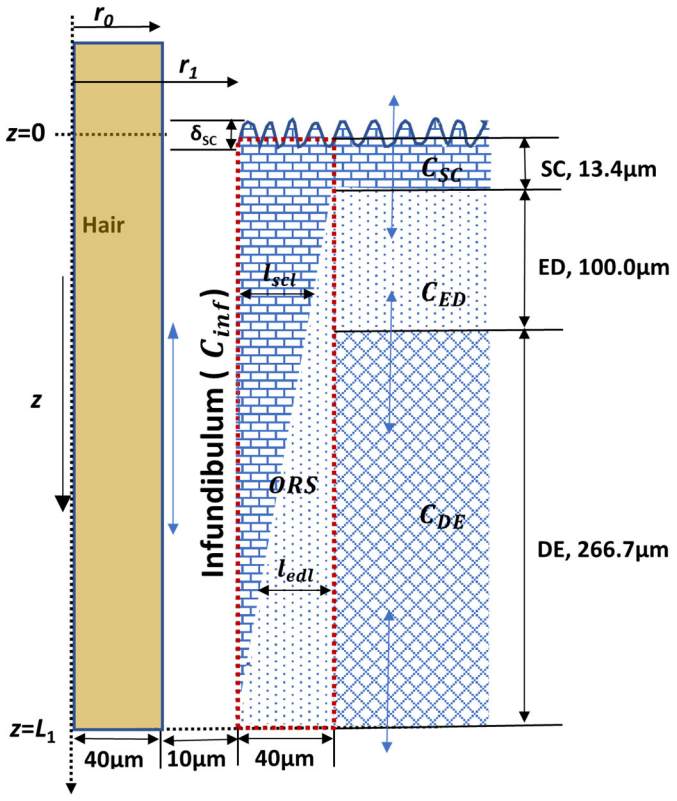

Figure 1. Schematic diagram of the follicular pathway (not to scale). The diagram shows a two-dimensional projection of a cylindrical hair follicle having an axis of symmetry at the left-hand boundary. Only the skin surface to the base of the infundibulum is depicted. Key dimensions l_{scl} and l_{edl} associated with the width of the SC-like and ED-like regions of the ORS are indicated, as is the surface roughness δ_{sc}. The hair shaft is considered to be impermeable. The base of the infundibulum is impermeable in the present simulations, but a fraction of "open" follicles can be included in the model.[4] The dashed red rectangle identifies the ORS region.

The permeability of the ORS is given by the standard bilaminate membrane formula combined with homogeneous membrane limits at the top and bottom of the infundibulum,[4]

$$P_{ors}(z) = \begin{cases} \frac{h_{sc}}{l_{scl}} P_{sc/w}^{comp} & 0 \le z \le h_{sc} \\ \left[\frac{1}{\frac{h_{sc}}{l_{scl}} P_{sc/w}^{comp}} + \frac{1}{\frac{h_{ed}}{l_{edl}} P_{ed}} \right]^{-1} & h_{sc} < z < L_1 \\ \frac{h_{ed}}{l_{edl}} P_{ed} & z = L_1 \end{cases} \quad (3a,b,c)$$

Here $P_{sc/w}^{comp}$ is the permeability of the interfollicular SC and P_{ed} is that of the viable epidermis (ED), h_{sc} and h_{ed} are the thicknesses of the interfollicular SC and ED, respectively, and L_1 is the total length of the follicular pathway.

In order to keep the model one-dimensional, lateral transport through the ORS in Model 2 was treated by including P_{ors} as a component of a mass transfer coefficient, k_{ors}, describing integrated solute transport across the ORS at depth z in the tissue,[4]

$$k_{ors}(z) = \frac{\frac{2r_1}{r_1^2 - r_0^2} P_{ors}(z)}{K_{inf/w}}, \quad (4)$$

as subsequently shown in Eq. 7a. This choice led to a small burst effect for permeation through the skin that was inconsequential in steady-state flux calculations, cf. Figure 4 of Yu et al. 2020.[4] But for small finite dose applications, the burst can indeed become significant. In order to put plausible limits on this phenomenon, we added a time lag to ORS flux based on Ash's multilaminate membrane analysis[15] and also the surface roughness feature described in the next section. A depth-dependent time lag for a bilaminate membrane, $T_{lag}(z)$,[15] (Eq. 5) is incorporated in Model 3 to calculate a time-delayed flux through the ORS membrane, $J_{ors}(z, t)$ (Eq. 6):

$$T_{lag}(z) = \left(\frac{l_{scl}}{D_{sc}} + K_{sc/ed} \frac{l_{edl}}{D_{ed}} \right)^{-1} \left[\frac{{l_{scl}}^2}{D_{sc}} \left(\frac{l_{scl}}{6D_{sc}} + K_{sc/ed} \frac{l_{edl}}{2D_{ed}} \right) + \frac{{l_{edl}}^2}{D_{ed}} \left(K_{sc/ed} \frac{l_{edl}}{6D_{ed}} + \frac{l_{scl}}{6D_{sc}} \right) \right] \quad (5)$$

$$J_{ors}(z,t) = \begin{cases} 0 & t \le T_{lag}(z) \\ P_{ors}\left[C_{inf}(z,t) - K_{inf/skin} C_{skin}(z,t) \right] & t > T_{lag}(z) \end{cases} \quad (6a,b)$$

Here D_{sc} and D_{ed} are diffusivities of the permeant in the SC and ED, respectively, and $K_{sc/ed}$ is the partition coefficient between SC and ED, calculated as $K_{sc/w} / K_{ed/w}$. $C_{inf}(z, t)$ is the concentration of permeant in the infundibulum, $C_{skin}(z, t)$ is the corresponding concentration in the adjacent skin layer and $K_{inf/skin}$ is the partition coefficient of the permeant between these two environments.[3]

Surface Roughness Limitation

In Model 2, lateral transport in the vehicle and each skin layer was considered to be rapid, so that each layer had a uniform concentration in the x-y plane, i.e. they were well-stirred. However, with decreasing volume of solution on the skin surface, we postulate that the vehicle film eventually breaks into small islands due to the surface roughness of the SC and potentially large interfacial energies. Consequently, in Model 3 lateral diffusion of solute in the vehicle is discontinued when the film thickness reaches a critical value, δ_{sc}. After this point, no more permeant is allowed to diffuse into the infundibulum. The volume of solution in the infundibulum begins to decrease due to solvent and solute transport across the ORS and to evaporation. In order to avoid undue complexity, the remaining solution is considered to be well stirred and to cling to the ORS as a uniform film. Therefore, the concentration of permeant in the infundibulum can be formulated as

$$\begin{cases} \frac{\partial C_{inf}(z,t)}{\partial t} = D_{inf}\frac{\partial^2 C_{inf}(z,t)}{\partial z^2} - k_{ors}(z)\left[C_{inf}(z,t) - K_{inf/skin}C_{skin}(z,t)\right] & h_v > \delta_{sc} \\ C_{inf}(z,t) = \mathrm{Min}\left(S_v, \frac{M_{inf}(t)}{V_{solution\_inf}(t)}\right) & h_v \le \delta_{sc} \end{cases} \quad (7a,b)$$

Here D_{inf} is the diffusivity coefficient of the solute in the infundibulum, and k_{ors} is the first-order exchange rate from infundibulum to each skin layer, cf. Eq. 4. When the vehicle thickness, h_v, is greater than the surface roughness (Eq. 7a), the infundibulum is assumed to be well stirred in the *xy* plane, but not in the *z* direction. When h_v falls below the surface roughness (Eq. 7b), the solution is assumed to be well stirred in all directions. S_v is the solubility of permeant in the solvent and

$M_{inf}(t)$ is the mass of solute in the infundibulum; it decreases over time as both solute and solvent absorb and evaporate. $V_{solution\_inf}$ is total volume of solution in the infundibulum. Equation 7b allows for precipitation of excess solute if its concentration in the solution exceeds S_v. The default value of δ_{sc} is taken to be 25μm, a typical value for the root mean square surface roughness of human skin.[16]

Dissolution Rate Limitation

It is evident from the data presented in the accompanying report[5] and also from existing literature[11,17,18] that the fate of dissolved chemicals following topical application to skin from volatile solvents depends upon both dose and the physicochemical properties of the test agent. Agents that are solids at skin temperature will precipitate on the skin if a sufficiently large dose is applied in the absence of a nonvolatile solvent. Absorption rate may subsequently be limited by the dissolution of this precipitate. This phenomenon has long been anticipated in theoretical descriptions of skin absorption,[10,19] and is generally described in terms of an interfacial diffusive resistance at the vehicle-skin interface. Yet there has been little attention paid to quantitatively describing this phenomenon. It bears much in common with the problem of solid-state stability of pharmaceutical actives, which has been the subject of extensive investigation over several decades.[20-22] The development below employs a one-layer diffusive resistance model predicated on the hypothesis that lipid solubility of the test agent will govern its dissolution kinetics following precipitation on the skin surface. Elaborations considering humidity-dependent remodeling of the deposited solid are possible,[20] but will not be considered here.

The physical model for the interfacial mass transfer resistance is shown in Figure 2. Although the diagram is drawn assuming solid particles with diameters comparable to a

micronized drug, a wide range of particle sizes may be anticipated. Quantifying this behavior and possible remodeling of the solids on skin is one of our long-term objectives.

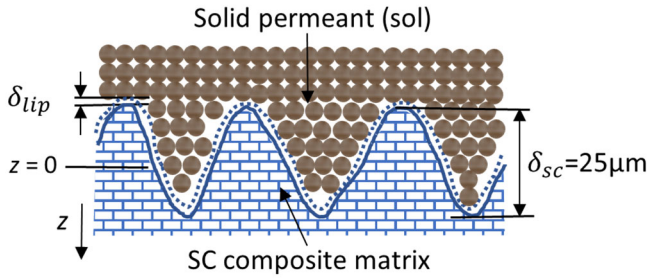

Figure 2. Schematic diagram for interfacial resistance at the vehicle-SC interface for a solvent-deposited solid. The diagram depicts small particles (d = ~3-5 μm) deposited on a skin surface with a root-mean-square roughness δ_{sc} = 25 μm. The interfacial resistance resides in the boundary layer δ_{lip} (dark blue line); its thickness and composition are discussed in the text. It is clear that the area of contact per unit area of skin, $f_{contact}$, will increase with increasing $\delta_{sc,}$, but decrease strongly with increasing d. This thinking accords with the well-known topical delivery benefits of micronized drug suspensions versus coarse suspensions.

Following the usual mass transfer approach for a thin interfacial lipid barrier having a thickness δ_{lip}, the flux per unit area A across the vehicle/skin interface (z = 0) is given by

$$J(0,\mathrm{t}) = \kappa_{lip}\left[C_{lip}\left(-\delta_{lip},t\right) - C_{lip}(0,t)\right] = \kappa_{lip}\left[S_{lip} - K_{lip/sc}C_{sc}(0,t)\right] \quad (8a)$$

$$= \kappa_{lip}\left[K_{lip/w}S_w - \left(\frac{K_{lip/w}}{K_{sc/w}}\right)C_{sc}(0,t)\right]. \quad (8b)$$

In Eq. 8a κ_{lip} is the interfacial mass transport coefficient, S_{lip} is the solubility of the dissolving solid in an interfacial (lipid) film having thickness δ_{lip}, and $K_{lip/sc}$ is the lipid/SC partition coefficient. C_{lip} and C_{sc} are concentrations of permeant at the lipid/SC interface. Eq. 8b recasts solubility and partition coefficients in terms of a linear partitioning isotherm, for ease of calculation. In the simplest picture, $\kappa_{lip} = \frac{D_{lip_{trans}}}{\delta_{lip}}$, where $D_{lip_{trans}}$ is the transverse diffusivity of the permeant in the film. We emphasize "transverse" to allow for the possibility that the lipid film could be comprised of anisotropic SC lipids,[23-25] and to distinguish it from the term "D_{lip}", which has been used to represent lateral diffusivity of the permeant in such lipids in earlier expositions of the SC composite matrix model, including Model 2.[3,23,24,26] Eq. 8 incorporates the assumption of partition

equilibrium at both the upper and lower boundaries of the film. In this form, it is entirely analogous to the Noyes-Whitney description of a solid particle dissolving into water.[27]

For solids deposited on the skin surface, we propose a modified interfacial mass transfer coefficient given by Eq. 9,

$$\kappa_{lip} = \left(\frac{D_{lip_{trans}}}{\delta_{lip}}\right) f_{contact} f_{thermo}. \quad (9)$$

Here, $f_{contact}$ is the fractional area of contact of the deposited drug per unit area of skin and f_{thermo} is a thermodynamic correction factor described under Data Analysis that corrects for changes in solute activity coefficient with concentration. Both factors are important for NA and MN, which are solids at skin temperature, yet are highly soluble in water and (for MN) lipids as well.

To make Eqs. 8 and 9 more concrete, one must specify the nature of the interfacial lipid film. What lipid(s) are involved? We consider two cases, human skin in vivo and excised human skin mounted in a diffusion cell (in vitro).

Human skin in vivo. In this case, the lipid film is likely to be sebaceous lipids, or more generally, skin surface film liquids (SSFL) as characterized by Stephaniak and Harvey.[28] According to this thinking, SSFL is comprised of remnants of sebaceous gland secretions and also sweat.[29] The thickness of such films in vivo is considered to be 1-4 μm, or even higher on the scalp.[29-31] Models for diffusivity and partitioning of solutes in sebum have been developed by Valiveti, Lu and coworkers.[32,33] Complementary models have been developed in conjunction with uptake of semivolatile organic compounds (SVOCs) from air.[34] Consequently, we recommend for in vivo exposures,

$$\kappa_{lip}^{in\ vivo} = \left(\frac{D_{SSFL}}{\delta_{SSFL}}\right) f_{contact} f_{thermo}. \quad (10)$$

where the values of D_{SSFL} and δ_{SSFL} may be estimated from the sebum values of Valiveti et al.[32,33]

Human skin in vitro. For in vitro exposures, evidence suggests that the SSFL film is completely removed;[3,35] however, the surface energy of SC in vitro is even less than that in vivo.[36] Ether-washed skin in vivo has also been shown to have lower surface energy than unwashed skin.[37] The implication is that excised human cadaver skin and ether-washed skin in vivo have a surface comprised of SC intercellular lipids, perhaps as little as the single covalently bound monolayer of lipid on the cornified cell envelopes. Adopting this hypothesis as a working model, we imbue the lipids with properties of SC lipids as described in Wang et al.,[24] i.e.

$$D_{lip_{trans}} \cong k_{trans} \cdot \delta \tag{11}$$

yielding

$$\kappa_{lip}^{in\ vitro} = \left(\frac{k_{trans}\delta}{\delta_{lip}}\right) f_{contact} f_{thermo}. \tag{12}$$

Here k_{trans} is the transverse mass transport coefficient across SC bilayer lipids and δ = 13 nm is the width of a single lipid bilayer. The predictive relationship for k_{trans} in partially hydrated skin used in Model 3 is that developed in Wang et al. (cf. their Model 2),[24] with the small modification to the leading coefficient (–2.725 => –2.730) described by Kasting et al. (see their Table 3 and note the change of units).[3]

$$\log_{10}[k_{trans}, \mathrm{m/s}] = -2.730 - 0.792\mathrm{MW}^{1/3} - \log_{10}(3) \tag{13}$$

The boundary conditions at the vehicle/SC interface can now be expressed in terms of the flux through the interfacial lipid film, $J(z, t)$, combined with evaporative loss from the vehicle (Eq. 14) and flux into the SC (Eq. 15) as follows:

$$\frac{dM_{surf}}{dt} = -k_{evap}\,\rho - J(-\delta, t) \tag{14}$$

$$-D_{\mathrm{sc}} \frac{\partial C_{sc}(z,t)}{\partial z}\Big|_{\mathrm{z=0}} = J(0,t) \tag{15}$$

where the value of $J(0,t)$is determined from Eqs. 8-13. For thin interfacial films we invoke the pseudo steady-state approximation, $J(-\delta,t) = J(0,t)$, so the boundary conditions at $z = 0$ are well posed.

For evaporation loss, the evaporation mass transfer coefficient k_{evap} is taken, after conversion to SI units, to be[38]

$$k_{evap} = k_g \frac{P_{vp}\mathrm{MW}}{\rho RT} \tag{16}$$

$$k_g = \frac{0.01756u^{0.78}}{\mathrm{MW}^{1/3}} \tag{17}$$

Here, k_{evap} and the gas phase mass transfer coefficient k_g are both expressed in m/s, ρ is the density of the solute in kg/m^3, u is the air velocity with a default indoor value of 0.165 m/s,[39] MW is molecular weight in kg/mol; P_{vp} is the vapor pressure for pure solute in Pa, R = 8.314 J·mol^{-1}K^{-1}, and T is the temperature of the skin surface in Kelvin (default value 305.15 K). The P_{vp} for solute in the liquid phase (or subcooled liquid phase) can be obtained from experimental data or from COSMOthermX prediction. When the melting point of solute (i.e. the fusion temperature T_f) is higher than skin temperature, the vapor pressure of pure solid solute $P_{vp}(\mathrm{solid})$ at the skin surface is estimated from Eq. (18),[40]

$$\ln\frac{P_{vp}(\mathrm{liquid})}{P_{vp}(\mathrm{solid})} = \frac{\Delta S_f}{RT}\left(T_f - T\right) \tag{18}$$

$$\Delta S_f = \begin{cases} \dfrac{\Delta H_f}{T_f} & \text{when } \Delta H_f \text{ is known} \\ 56.5\ \mathrm{jK^{-1}mol^{-1}} & \text{when } \Delta H_f \text{ is unknown} \end{cases} \tag{19}$$

The evaporation model in Eqs. 16-19 applies to both in vitro and in vivo exposures, although the appropriate air velocity u may vary. Using the approximations in Eqs. 13 and 16-19, the only unknown parameter in the solute mass transfer at the skin surface is κ_{lip}.

The breakdown of $\kappa_{lip}^{in\ vitro}$ into four separate factors (Eq. 12) is not necessary to model the experimental data, as a single value of $\kappa_{lip}^{in\ vitro}$ will be selected for each compound, NA and MN. But it is helpful for think about this mass transfer coefficient in terms of molecular and cooperative properties to understand the basis for what will be shown to be an enormous difference in $\kappa_{lip}^{in\ vitro}$ for NA and MN. The factors $k_{trans}\delta$ and f_{thermo} are determined independently from the skin permeation data, so that the other two factors, δ_{lip} and $f_{contact,}$ can be tentatively determined from the two independent skin permeation datasets. The way this was done is described later.

Materials and Methods

Physical Properties of Test Permeants

The physical properties relevant to the present analysis were obtained and discussed in the companion report[5] and are summarized in Table 1. Additional properties related to aggregation of NA in aqueous solution and the resulting impact on K_{ow} are discussed elsewhere.[41] The salient properties related to the present analysis are: (1) NA and MN are highly soluble in water, and MN is also highly soluble in lipids; (2) NA associates strongly in aqueous solutions; (3) K_{ow} for both compounds is a decreasing function of concentration; and (4) NA forms highly crystalline deposits following solvent deposition, whereas MN deposits as a supercooled liquid or amorphous solid.[5]

Table 1. Physicochemical properties of the test solutes

Permeant	MW g/mol	Density[a] g/L	mp °C	log K_{ow}	P_{vp} Pa	S_w g/L[b]	S_{oct} g/L[b]
Niacinamide	122.13	1277	130[c]	-0.37[c] -1.39[e]	0.01[d]	534	21.6
Methyl nicotinate	137.14	1156	42.5[c]	0.83[c] 0.31[e]	31[d]	372	759

[a] Supercooled liquid density at 32°C, predicted by COSMOthermX
[b] 30°C[5]
[c] Source: PubChem[42]
[d] COSMOthermX prediction at 32°C
[e] Saturated solution value estimated as log [S_{oct}(g/L) / S_w(g/L)][5]

In Vitro Permeation Studies (IVPT)

These studies are fully described in the companion report.[5] NA and MN permeation through excised human skin mounted in Franz diffusion cells after solvent deposition from 1:1 ethanol:water solutions was measured over a dose range spanning 4.5 orders of magnitude.

Data Analysis

Thermodynamic Correction Factor. NA is known to associate in aqueous solution,[43,44] whereas less is known regarding MN. NA is also likely to associate in the corneocyte phase of the SC, which is water-continuous, although details may be modified by binding of both water[45] and NA[46] to keratin and also the presence of other solutes such as natural moisturizing factor components.[47] A full treatment of NA thermodynamic activity within the SC is furthermore complicated by the fact that concentration-dependent activity coefficients lead to variable diffusivity and variable lipid/water partition coefficients within the tissue.[48] We considered and discarded the idea of conducting such an analysis due to concerns regarding the lack of tissue-specific data and the extra effort involved with solving the nonlinear equation system. As an alternative, we chose the simpler approach of considering NA activity in the vehicle phase only, and applying a thermodynamic correction factor, f_{thermo} (cf. Eq. 12), at the vehicle-interfacial film interface. Based on the concentration-dependent partition coefficients in Table 1 we obtained $f_{thermo} = K_{ow}$ (sat) / K_{ow} (dilute) = 0.095 for saturated solutions of NA in the vehicle and for precipitated NA resting on the interfacial lipid film. For MN, we used the same procedure to obtain $f_{thermo} = 0.30$.

Simulations and parameter estimation. Physical properties of NA and MN described earlier were used as inputs to the modified finite dose simulation model (Model 3). Skin surface temperature was set to 32°C and airflow over the diffusion cells to 0.165 m/s (finite dose only).[39] Both steady-state permeability and finite dose skin permeation rate were calculated. The former employed the

fully hydrated skin model; the latter employed partially hydrated skin.[24,26] After experimenting with Model 2^4 to develop the refinements discussed above, three sets of final calculations were performed:

1. Default permeation rates for Model 3 were simulated using either no adjustable parameters (steady state) or one adjustable parameter (finite dose). For the latter, a single value for the vehicle-skin mass transfer coefficient, κ_{lip} (Eq. 9) was used across doses to best describe the dose-dependence of NA and MN permeation.
2. Model 3 was fitted to the experimental permeation rates using one (steady state), two (finite dose, NA), or three (finite dose, MN) adjustable parameters. For the steady-state fits, the value of the transverse mass transfer coefficient across the SC lipids, k_{trans} (Eq. 13), was varied to best match the average permeation rates. For finite dose NA, the values of k_{trans} and κ_{lip} were varied. For finite dose MN, the values of k_{trans}, κ_{lip} and the solute vapor pressure, P_{vp}, were varied to simultaneously match the initial permeation rates and the plateau values of absorption after prolonged exposures. For MN doses that reached a plateau, unabsorbed solute was considered to have evaporated. NA was essentially nonvolatile but permeated so slowly that an absorption plateau was not reached at any dose tested. Rather than separately fitting the mean data for each of the two NA donors, one set of parameters was developed that yielded cumulative permeation matching the average of the two datasets.
3. The above calculations (without κ_{lip}) were repeated using the Excel®-based UB/UC model[26] in order to determine how much model predictions had changed for these two solutes since publication of the much simpler model in 2013.

The parameters selected for optimization were chosen because of their dominant effects on dissolution rate (κ_{lip}), initial skin permeation rate (k_{trans}) and evaporation rate (P_{vp}). In each case, a change in the parameter value resulted in a nearly proportional change in the respective transport rate. Optimization was done manually by examination of cumulative permeation graphs. Because each finite dose dataset consisted of 72-81 observations covering 9 doses and 8-9 collection times, and each observation was itself an average over 6-11 skin replicates, it was possible to adjust these parameters without overfitting the dataset.

Results

Steady-state permeability (k_p)

Experimental and predicted steady-state permeabilities for NA and MN are shown in Table 2, and example permeation profiles for NA are shown in Figure 3. The mean permeability coefficient of MN was 70-fold higher than that of NA, a remarkable difference for two compounds of comparable molecular size and a 16-fold difference in octanol/water partition coefficient (MN > NA). The Potts-Guy relationship,[49] for example, predicts a 5.8-fold difference in k_p (Table 2), whereas UB/UC and Model 3 predict ratios of slightly over 6. The NA experiments were conducted with a donor solution concentration of 10 μg/mL (8.2×10^{-5} M), well under the concentration range where aggregation in aqueous solutions impacts the activity coefficient.[41]

Table 2. Experimental and predicted k_p values for NA and MN from aqueous solutions through excised human skin. Simulations assumed fully hydrated skin, T = 32°C and f_{open} = 0.

	$k_p \times 10^{10}$, m/s				k_{trans} multiplier[a]		
Permeant	Experimental	Potts-Guy[49]	UB/UC[2,6]	Model 3	Potts-Guy	UB/UC	Model 3
NA	1.36 ± 1.31[b]	5.44	4.67	5.36	0.25	0.29	0.25
MN	96.1 ± 11.1[c]	31.4	30.0	33.3	3.1	3.2	2.9

[a] Factor by which the default value of k_{trans} must be multiplied to match experimental k_p value. Default values of k_{trans} for fully hydrated SC are 2.22×10^{-7} m/s for NA and 1.55×10^{-7} m/s for MN.
[b] (n = 5 donors, 31 replicates)[50]
[c] (n = 2 concentrations 5-10 replicates);[51] (n = 1, 3 replicates)[52]

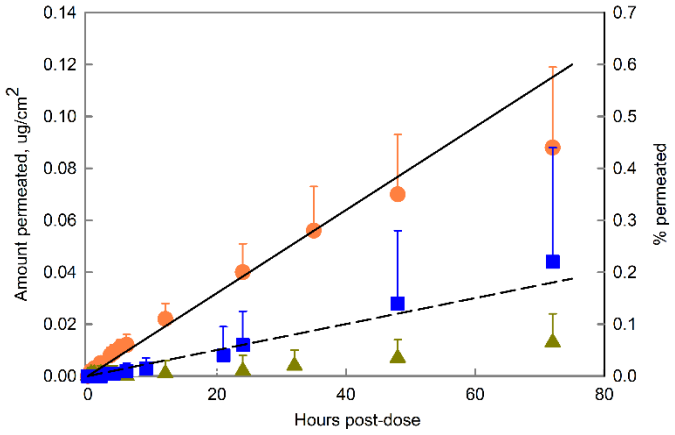

Figure 3. Permeation of niacinamide (NA, 10 µg/mL in water) across freshly excised human epidermal membrane from 3 surgical skin donors. Each symbol represents the geometric mean + SE for one donor, n = 5-8 samples/donor. The mean permeability coefficient, k_p, calculated from the linear regions for 5 skin donors (n = 31 total) is reported in Table 2. Calculated permeation based on the mean k_p is shown as a dashed line and the default prediction from Model 3 as a solid line. Skin temperature was 30-32°C. The data are from Ref. 50.

The MN experiments of Dal Pozzo et al.[51] were conducted at 50-100 mg/mL (0.36-0.73 M), concentrations at which skin penetration enhancer activity could conceivably come into play; however, we are not aware of enhancer activity reported for MN in vitro, where blood flow is not a factor. Test concentrations of MN were not specified in the study by Degim et al.[52]

It is evident from Table 2 and Figure 3 that in vitro steady-state skin permeation for NA shows considerable inter-donor and intra-donor variability, much more so than MN. This occurred despite the fact that the steady-state NA permeation experiments were conducted in freshly excised surgical skin samples that had all passed a ^3H_2O permeation test.[50,53] The higher variation in skin permeability for poorly penetrating, hydrophilic permeants is consistent with our own experience and that of others.[54] It will be seen again in the finite dose permeation studies described below.

Finite dose skin permeation

Figure 4 shows cumulative permeation of NA at a very low dose (Fig. 4a) and a very high dose (Fig. 4b), along with the best model fits across all doses for UB/UC,[26] Model 2[4] and Model 3.

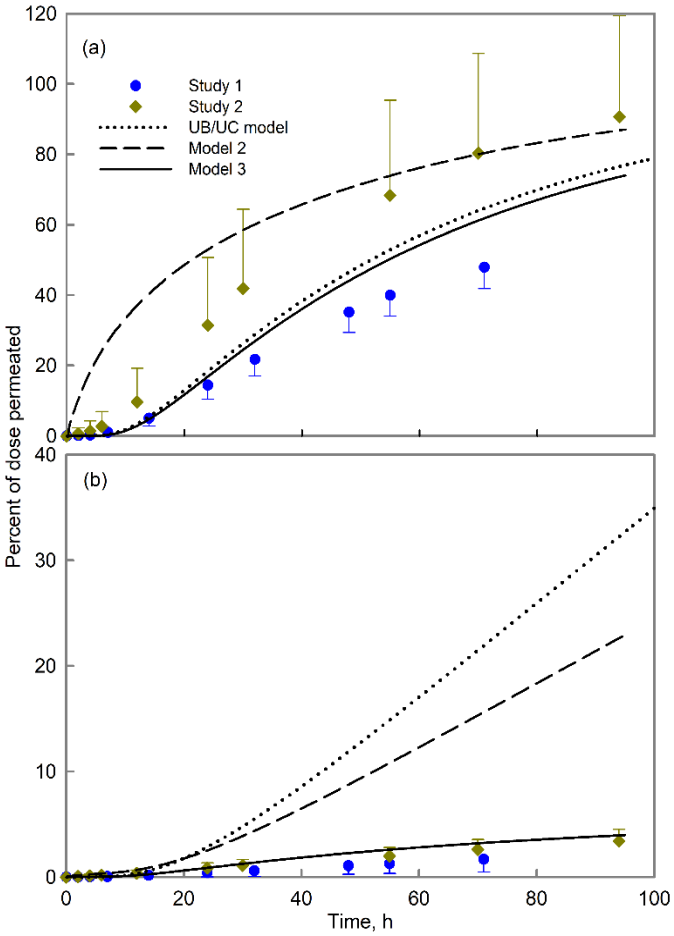

Figure 4. Predicted and experimental human skin penetration for NA at applied doses of (a) 2 µg/cm^2, and (b) 2741 µg/cm^2. The lines represent model predictions and symbols show the experimental values.

UB/UC was effective at the low dose, but substantially overpredicted permeation at the high dose. Model 2 overpredicted permeation at both doses. The rapid early permeation for the low dose resulted from two factors associated with the follicular delivery component: failure to include a time lag for permeation through the outer root sheath (ORS) and strict adherence to the well-stirred vehicle assumption, which allowed excessive solute to accumulate in the follicles as the vehicle

dried down. At high doses the follicular component was inconsequential, but the lack of a dissolution limitation led to overprediction of absorption. Model 3 was equivalent to UB/UC at the low dose, but also closely matched the high dose permeation data. All four refinements described in the Mathematical Model section were required to obtain the Model 3 results. A similar scenario was incurred for MN, although the dissolution mass transfer coefficient was much larger. Fitted parameters associated with Model 3 are shown in Table 3, and the full set of simulated permeation profiles for NA and MN are shown in Figures 5 and 6, respectively.

Table 3. Parameters associated with fits of UB/UC and Model 3 to the NA and MN permeation data in Ref. 5. Simulations assumed partially hydrated skin, T = 32°C and f_{open} = 0. Brackets denote a parameter that was fixed at the value estimated in the text.

Parameter	Equation	NA		MN	
		UB/UC	Model3[a]	UB/UC	Model3
$\kappa_{lip} \times 10^{12}$, m/s	9	-	3.65, 9.84	-	1330
$k_{trans}\delta \times 10^{16}$, m^2s^{-1}	11		4.75, 6.17[b]		66.4[b]
$f_{contact}/\delta_{lip} \times 10^{-5}$, m^{-1}	9, 12	-	0.81, 1.68 [c]	-	6.63 [c]
f_{thermo}	9, 13	-	[0.095]	-	[0.30]
k_{trans} multiplier[d]	12, 13	0.40	0.50, 0.65	10	10
P_{vp} multiplier[e]	16	-	-	1.8	0.44

[a] The two values in this column refer to Studies 1 and 2, respectively.

[b] Default value of $k_{trans}\delta$ (Eq. 11) multiplied by k_{trans} multiplier in Line 5. Not independently fit.

[c] Value derived from κ_{lip}, $k_{trans}\delta$ and f_{thermo} according to Eq. 12. Not independently fit.

[d] Factor by which default value of k_{trans} must be multiplied to achieve the optimum fit. Default values for partially hydrated skin are 7.30×10^{-8} m/s for NA and 5.11×10^{-8} m/s for MN. Both are 1/3rd of the hydrated skin value.[24]

[e] Factor by which default value of P_{vp} (Table 1) must be multiplied to achieve the optimum fit.

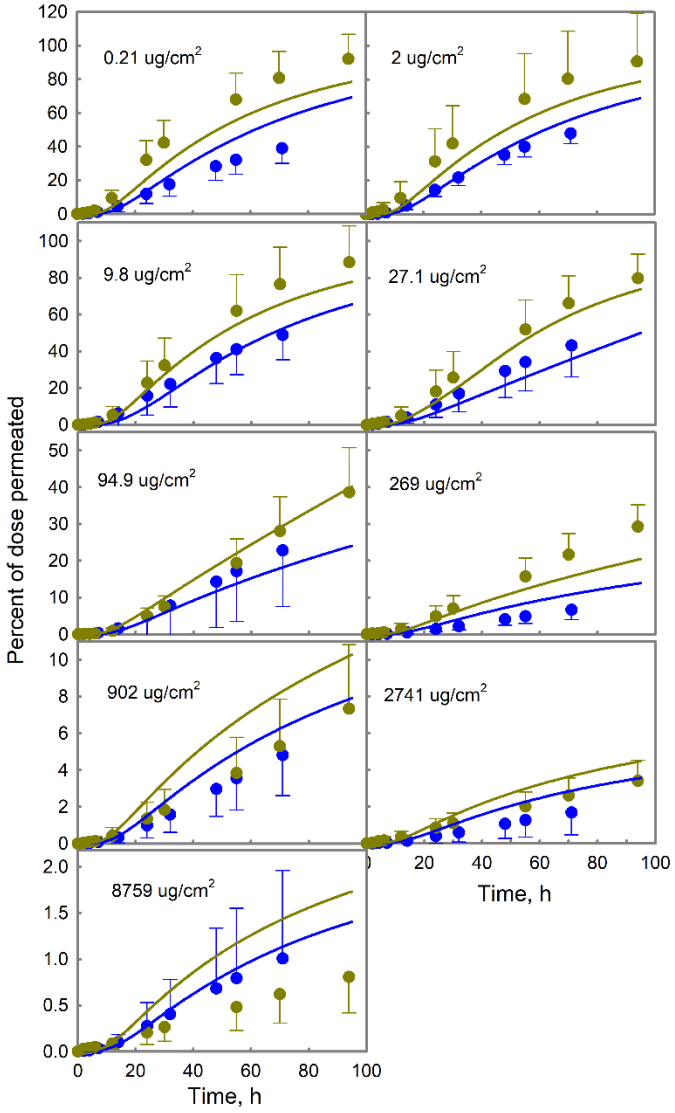

Figure 5. Model 3 predictions versus cumulative permeation of NA from 9 finite doses following solvent deposition on human skin in vitro. The data are from Ref. 5. The numbers at the top left of each graph reflect the dose in μg/cm^2. Blue and tan symbols represent Studies 1 and 2, respectively, and the solid lines represent fits to these datasets.

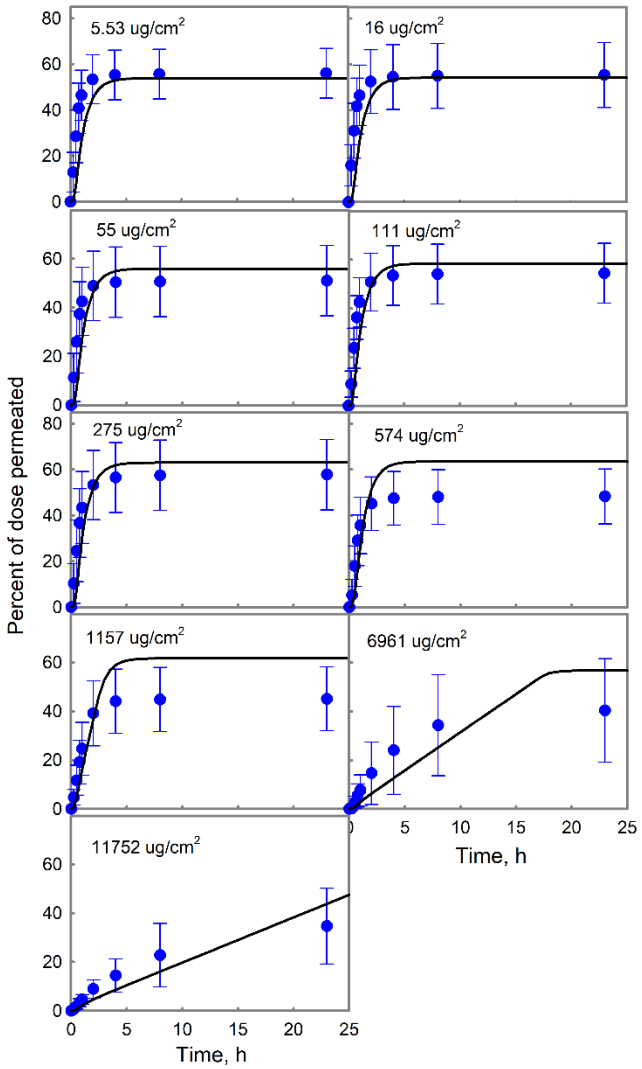

Figure 6. Model 3 predictions versus cumulative permeation of MN from 9 finite doses following solvent deposition on human skin in vitro. The data are from the companion report.[5] The numbers appearing on the graphs reflect the dose in μg/cm^2.

Discussion

Although the general pattern of dose-dependent dermal absorption for NA and MN is a familiar one,[2] the difference in rate of absorption between the two compounds is striking. Whether in dilute aqueous solutions (Fig. 3, Table 2) or solvent-deposited onto the skin (Figs. 5 & 6, Table 3) MN absorption rate through excised human skin exceeds that of NA by a factor of 60-70. Both model extensions and parameter adjustments were required to match the full range of in vitro skin

absorption data obtained in these studies. The comments that follow classify these modifications according to the major feature impacted by the change.

Initial absorption rates and steady-state permeability

Using default model parameters, the current (Model 3) and earlier (UB/UC, Model 2) finite dose absorption models from our group predict the direction, but not the magnitude, of the difference in absorption rates between these compounds. NA absorption rates are overpredicted, but MN absorption rates are substantially underpredicted. The same can be said for widely-accepted steady-state models of skin permeability including that of Potts and Guy,[49] as shown in Table 2. In all models discussed, the dominant factor governing skin permeability for moderately hydrophilic or lipophilic permeants is diffusive resistance of the SC lipids in a direction transverse to the plane of the membrane. In Potts and Guy, it is the *only* factor. This resistance can be thought of as $h_{lip}/(D_{trans}K_{lip})$, where the factors refer, respectively, to lipid thickness and the (transverse) diffusivity and partition coefficient of the permeant in these lipids. In UB/UC and subsequent models discussed here, $D_{trans} \cong k_{trans} \cdot \delta$, where k_{trans} is a mass transfer coefficient and δ is the average thickness of an intercellular lipid layer.[24] On the premise that our existing estimates of h_{lip}, K_{lip} and δ are reliable,[23,24,55] we varied k_{trans} in order to match the steady state permeation rates (infinite dose) or the initial permeation rates of NA and MN at low, finite doses. Results were expressed as a multiplier that must be applied to the default k_{trans} value to match the data. These values are shown in Table 2.

UB/UC and Model 3 yielded comparable k_{trans} multipliers for NA and MN steady-state permeation rates (0.25-0.29 for NA, 2.9-3.2 for MN), indicating that the models predicted steady-state permeabilities in hydrated skin to within a factor of 3-4. The multipliers for Model 3 were 10-14% lower than for UB/UC, which is fully explained by the follicular contribution discussed

later. These departures of model predictions from experiment are reminiscent of root-mean-square estimates of variability in steady-state predictions in the original SC model of about $10^{0.52} = 3.3$.[24] But what is considered acceptable agreement on a log-log plot is often disappointing on a linear scale. There is room for improvement in the prediction.

For finite doses, NA initial absorption rates were overpredicted by about a factor of two, yielding k_{trans} multipliers of 0.40-0.65, whereas MN absorption rates were underpredicted by a factor of 10 (Table 3). The k_{trans} multipliers cited here are based on the partially hydrated skin limit of both UB/UC and Model 3. Higher skin concentrations are achieved in the finite dose studies due to the concentrated deposits that form on the skin surface during dry down. It is possible that interaction of MN with SC lipids increased its permeability at these high skin concentrations, leading to more rapid permeation through the skin.

Evaporation rates

Cumulative absorption of MN in the finite dose studies reached a plateau value of 48-60 percent of dose for all but the two highest doses (Fig. 5). By assuming missing material to have evaporated, an evaporation rate can be estimated according to Eqs. 16-19. Because the diffusion cells and test environment were similar to those used in separate calibration studies,[56] we considered that the most uncertain value in the evaporation rate calculation was the permeant vapor pressure, P_{vp}, for which only an estimate for the subcooled liquid was available (Table 1). Consequently, we expressed the departures from default parameter predictions as the P_{vp} multiplier required to match the cumulative absorption plateau values at low MN doses (Table 3). In this instance, the optimum P_{vp} multiplier for UB/UC and Model 3 were quite different, i.e. 1.8 and 0.44, respectively. This difference can be understood based on model architecture. UB/UC does not explicitly consider the solvent in a solvent deposition study. Permeant is immediately deposited

in the upper SC layers (the "deposition zone"[38]) and the skin surface (once the deposition zone is saturated). Model 3 involves an explicit evaporation and absorption process for the solvent, so dilute solutions of a volatile permeant evaporate much more slowly due to the lower vapor pressure of the solute above the solution. At higher applied doses, the dissolution limitation in Model 3 comes into play (Eqs. 8-12). The factor $\kappa_{lip}^{in\ vitro}$ (Eq. 12) limits the absorption of MN, so that a lower evaporation rate is required to match the plateau observed in MN absorption up to doses of about 1200 μg/cm^2 (Fig. 6). This factor is discussed in the next section.

With a vapor pressure of about 0.01 Pa (Table 1), NA is effectively a nonvolatile permeant; hence P_{vp} does not play a role in its disposition on skin.

Dissolution limitation

It is evident from Figure 4 and the above discussion that neither UB/UC nor Model 2 were able to quantitatively describe either NA or MN absorption over the full dose range of the studies. This finding prompted the introduction of the dissolution mass transfer coefficient κ_{lip} in Eq. 8 and the further factorization of κ_{lip} in Eqs. 9-12. It was furthermore evident that κ_{lip}(NA) must be much less than κ_{lip}(MN) for this construct to work. The area of contact factor $f_{contact}$ was introduced to provide this distinction.

Support for such a factor appears in Table 1 and the companion report.[5] MN is a low-melting solid with high solubility in octanol. NA is a high-melting solid with limited solubility in octanol. Considering proposed Model 3 relationship for SC lipids,[55] $K_{lip/w}$ =0.35 $(K_{oct/w})^{0.81}$, it is reasonable to postulate that the octanol solubility differences carry over into SC lipids.

Furthermore, the melting point difference suggests possible crystallinity differences at skin temperature, which are confirmed by crossed polar optical microscopy.[5] Let's consider the fitted parameter $f_{contact}/\delta_{lip}$ reported in Table 3, and furthermore assume that the value of δ_{lip} is the

same for NA and MN. If one considers that the value of $f_{contact}$ = 1 for MN, an amorphous solid or perhaps supercooled liquid permeant, then the value of δ_{lip} must be $1/(6.63 \times 10^5\ m^{-1}) = 1.51 \times 10^{-6}$ m = 1.51 μm. This value is comparable to the 1-4 μm thickness of sebum films on human skin in vivo and approximately 20 times thicker than the typical 0.075 μm thickness of intercellular SC lipids.[24] Considering the argument associated with Eqs. 11 and 12, and also found in Ref. 4, that the sebum film is completely removed from cadaver skin prepared by tissue banks, such a thick film seems highly unlikely. If one makes the alternative assumption that δ_{lip} = 0.075 μm, then $f_{contact} = (6.63 \times 10^5\ m^{-1})(0.075 \times 10^{-6}\ m) = 0.050$ for MN and an average of $(1.25 \times 10^5\ m^{-1})(0.075 \times 10^{-6}\ m) = 0.0094$ for NA. In either case the fractional contact area for MN deposited on the skin surface is approximately 5-fold that of NA. We plan to continue our investigation of the factors impacting κ_{lip} by studying additional permeants, solvents and substrates.

An alternative way of thinking about mass transfer at the solid-skin interface in vitro is that the initial mass transfer rate is proportional to $\kappa_{lip} \cdot S_{lip}$ (Eq. 8a) or, equivalently, to $(k_{trans} \cdot \delta) \cdot f_{contact} \cdot S_{lip}$. Thus, compounds with high diffusivity and solubility in SC lipids and low crystallinity (like MN) will have higher mass transfer rates following solvent deposition. We tentatively classify MN as a "soft solid" and NA as a "hard solid" based on this distinction. A quantitative and continuous scale connecting these limits requires the study of additional materials having intermediate properties.

Polar pathway and follicular diffusion

The inability of the UB/UC model to correctly predict the dermal absorption of ionized compounds or other highly hydrophilic species has been justifiably viewed as a significant limitation.[57,58] Considerable effort to address this issue led to the development of a method to incorporate a "polar pathway" within the UB/UC framework, which to date has been discussed

only in the context of steady-state skin permeability.[3,4] The most influential component of the proposed polar pathway for most exposure scenarios is the follicular pathway, which was first outlined in Kasting et al.[3] and subsequently refined in Yu et al.[4] The latter version is termed here "Model 2".

Upon applying Model 2 to analyze the present finite dose datasets, we quickly found that follicular transport had to be dialed back in a significant manner (Fig. 4). Approximations that sufficed in the steady state led to unrealistically high absorption rates for permeants applied from volatile solvents at very low doses. This resulted from the lack of a time lag for permeant entering the skin through the follicular ORS and the propensity of the well-stirred vehicle approximation to allow an enormous fraction of dissolved solute to accumulate in the follicular infundibulum as the solvent dried down. Experimental studies of follicular delivery establish that this does not happen.[59] The time lag and surface roughness limitations described in the Mathematical Model section address these issues. A third feature of Model 2, regarding a small fraction of follicles open to the receptor solution (1.5% in Model 2), could have presented a problem, but it became inconsequential in the present analysis once the first two limitations were introduced. We assumed no open follicles ($f_{open} = 0$) in the present simulations.

Once the above modifications had been incorporated into Model 3, the presence of a follicular diffusion pathway had little impact on the diffusion model's ability to accurately simulate finite dose permeation of the two compounds examined in this study. This can be seen by the agreement of the optimized predictions arising from UB/UC and Model 3 at low doses (Figs. S1 and S2). This agreement was obtained despite steady-state calculations indicating a follicular contribution to permeation of 10% for MN and 14% for NA, cf. the discussion related to Table 3. Very different results would be found for highly hydrophilic permeants, such as sugars and sugar

alcohols, inorganic ions or highly ionized weak electrolytes. Dermal absorption predictions related to topical exposures to permeants in these categories, e.g. lead salts, paraquat or (possibly) diclofenac sodium, could be highly influenced by the presence or absence of a follicular pathway.

Outlook

The development reported here extends the domain of mechanistic skin penetration modeling to finite dose exposures of solvent-deposited solids over a wide dose range. As we generalize our approach to other permeants, vehicles and exposure conditions, we expect additional model components will be required. For example, for compounds more lipophilic than NA and MN, the potential impact of slowly reversible binding to keratin must be considered.[60,61] Furthermore, we note that the impact of vehicle components and form on skin permeability is still relatively unexplored from a mechanistic viewpoint, although commercially available software already offers some capability.[62-64] Continuously improving methods for molecular simulations of structured lipids offer promise in this area.[64-66] Notably, at least one method offers the capability for non specialists to mechanistically study the impact of solute-membrane interactions on membrane permeability.[64,66] Considering that the Model 3 prediction of the underlying membrane permeability of moderately lipophilic solutes in the SC has not improved substantially since Potts and Guy's 1992 correlation[49] (c.f. Table 2), there is ample room for improvements in this area. We view this as an opportunity for molecular modelers as well as commercial software developers to make major contributions to predictive skin permeation models.

We are humbled by the amount of effort required to reliably implement each new development. But these developments are ultimately shareable. The UB/UC model was released as the NIOSH Finite Dose Permeation Calculator as early as 2011[67] and now serves as the dermal input module to PKSim™, an open access PBPK platform downloadable from the web.[68]

Restriction of the present model to a one-dimensional architecture enables the possibility of encoding it as a system of finite difference equations in space and ordinary differential equations (ODEs) in time suitable for direct implementation on simultaneous ODE solvers.

Conclusions

The ex vivo human skin absorption of two closely related topical agents, NA and MN, following solvent deposition has been characterized experimentally and described in terms of a mechanistic transient diffusion model. The model reveals insights into the striking difference in absorption rate of the two compounds based on vastly different dissolution or release rates from the deposited solid. It also highlights the importance of solute/SC lipid interactions in determining skin permeation rates. The mechanistic model offers a quantitative explanation for practical guidance from an earlier generation of pharmaceutical scientists: "In general, an efficacious topical gel formulation is one in which: (a) the concentration of diffusible drug in the vehicle…is optimized by ensuring that all of the drug is in solution, (b) the minimum amount of solvent is used to dissolve the drug completely…, and (c) the vehicle components affect the permeability of the stratum corneum in a favorable manner."[69]

Interests

Niacinamide is a skin care ingredient included in certain Procter & Gamble products. JJ is an employee of the Procter & Gamble Company. The modeling study was conducted to improve predictive models for dermal absorption of topically applied compounds, an objective shared by Procter & Gamble and the University Cincinnati through their joint involvement with CBET grant #2124495, an NSF GOALI project also including Prof. J. M. Nitsche at the University of Buffalo.

Acknowledgements

FY and KT acknowledge support from the Procter & Gamble Company. LX was supported by a graduate assistantship from the University of Cincinnati. GBK received support from an internal grant from the JLW College of Pharmacy and from NSF grant #2124495 (CBET).

References

1. Mitragotri S, Anissimov YG, Bunge AL, Frasch HF, Guy RH, Hadgraft J, Kasting GB, Lane ME, Roberts MS 2011. Mathematical models of skin permeability: An overview. Int J Pharm 418:115-129.
2. Frasch HF, Bunge AL, Chen C-P, Cherrie JW, Dotson GS, Kasting GB, Kissel JC, Sahmel J, Semple S, Willkinson S 2014. Analysis of finite dose dermal absorption data: implications for dermal exposure assessment. J Expos Sci Environ Epidem 24:65-73.
3. Kasting GB, Miller MA, LaCount TD, Jaworska J 2019. A composite model for the transport of hydrophilic and lipophilic compounds across the skin. J Pharm Sci 108:337-349.
4. Yu F, Tonnis K, Kasting GB, Jaworska J 2020. Computer simulation of skin permeability of hydrophobic and hydrophilic chemicals: Influence of follicular pathway. J Pharm Sci 110:2149-2156.
5. Kasting GB, Miller MA, Xu L, Yu F, Jaworska J 2021. In vitro human skin absorption of solvent-deposited solids: niacinamide and methyl nicotinate. J Pharm Sci in press.
6. Bissett DL, Miyamoto K, Sun P, Li J, Berge CA 2004. Topical niacinamide reduces yellowing, wrinkling, red blotchiness, and hyperpigmented spots in aging facial skin. Int J Cosmet Sci 26:231-238.
7. Tanna O, Ota Y, Kitamura N, Katsube T, Inoue S 2000. Nicotinamide increases biosynthesis of ceramides as well as other stratum corneum lipids to improve epidermal permeability barrier. Brit J Dermatol 143:524-531.
8. Guy RH, Carlstrom EM, Bucks DAW, Hinz RS, Maibach HI 1986. Percutaneous penetration of nicotinates: In vivo and in vitro measurements. J Pharm Sci 75:968-972.
9. Tur E, Maibach HI, Guy RH 1991. Percutaneous penetration of methyl nicotinate at three anatomic sites: Evidence for appendageal transport? Skin Pharmacol 4:230-234.
10. Anissimov YG, Roberts MS 2001. Diffusion modeling of percutaneous absorption kinetics: 2. Finite vehicle volume and solvent deposited solids. J Pharm Sci 90:504-520.
11. Scheuplein RJ, Ross LW 1974. Mechanism of percutaneous absorption V. Percutaneous absorption of solvent deposited solids. J Invest Dermatol 62:353-360.
12. Crutcher W, Maibach HI 1969. The effect of perfusion rate on in vitro percutaneous penetration. J Invest Dermatol 53:264-266.
13. Knorr F, Lademann J, Patzelt A, Sterry W, Blume-Peytavi U, vogt A 2009. Follicular transport route - Research progress and future perspectives. Eur J Pharm Biopharm 71:173-180.
14. Patzelt A, Lademann J 2013. Drug delivery to hair follicles. Exp Opin Drug Deliv 10:787-797.
15. Ash R, Barrer RM, Palmer DG 1965. Diffusion in multiple laminates. Brit J Appl Phys 16:873-884.

16. Tchvialeva L, Zeng H, Markhvida I, McLean DI, Lui H, Lee TK. 2010. Skin roughness assessment. In Campolo D, ed New Developments in Biomedical Engineering, London, UK: IntertechOpen. pp 341-358.

17. Feldmann RJ, Maibach HI 1970. Absorption of some organic compounds through the skin in man. J Invest Dermatol 54:399-404.

18. Hewitt NJ, Grégoire S, Cubberley R, Duplan H, Eilstein J, Ellison C, Lester C, Fabian E, Fernandez J, Géniès C, Jacques-Jamin C, Klaric M, Rothe H, Sorrell I, Lange D, Schepky A 2019. Measurement of the penetration of 56 cosmetic relevant chemicals into and through human skin using a standardized protocol. J Appl Toxicol 2019:1-13.

19. Albery WJ, Hadgraft J 1979. Percutaneous absorption: interfacial transfer kinetics. J Pharm Pharmacol 31:65-68.

20. Carstensen JT, Po ALW 1992. The state of water in drug decomposition in the moist solid state: Description and modeling. Int J Pharm 83:87-94.

21. Carstensen JT, Danjo K, Yoshioka S, Uchiyama M 1987. Limits to the concept of solid-state stability. J Pharm Sci 76:548-550.

22. Carstensen JT. 1977. Pharmaceutics of Solids and Solid Dosage Forms. New York: Academic Press.

23. Wang T-F, Kasting GB, Nitsche JM 2006. A multiphase microscopic model for stratum corneum permeability. I. Formulation, solution and illustrative results for representative compounds. J Pharm Sci 95:620-648.

24. Wang T-F, Kasting GB, Nitsche JM 2007. A multiphase microscopic model for stratum corneum permeability. II. Estimation of physicochemical parameters and application to a large permeability database. J Pharm Sci 96:3024-3051.

25. Barbero AM, Frasch HF 2017. Effect of stratum corneum heterogeneity, anisotropy, asymmetry and follicular pathway on transdermal penetration. J Control Rel 260:234-246.

26. Dancik Y, Miller MA, Jaworska J, Kasting GB 2013. Design and performance of a spreadsheet-based model for estimating bioavailability of chemicals from dermal exposure Adv Drug Deliv Revs 65:221-236.

27. Sinko PA. 2011. Martin's Physical Pharmacy and Pharmaceutical Sciences. 6th ed., Philadelphia, PA: Lippincott Williams & Wilkins.

28. Stefaniak AB, Harvey CJ 2006. Dissolution of materials in artificial skin surface film liquids. Toxicol in Vitro 20:1265-1283.

29. Stefaniak AB, Harvey CJ, Wertz PW 2010. Formulation and stability of a novel artificial sebum under conditions of storage and use. Int J Cosmet Sci 32:347-355.

30. Baalbaki NH, Kasting GB 2017. Evaluating the transport kinetics of a model compound released from cellulosic coacervate compositions into artificial sebum. J Pharm Sci 106:1578-1585.

31. Sheu HM, Chao SC, Wong TW, Lee YY, Tsai JC 1999. Human skin surface lipid film: an ultrastructural study and interaction with corneocytes and intercellular lipid lamellae of the stratum corneum. Brit J Dermatol 140:385-391.

32. Valiveti S, Lu GW 2007. Diffusion properties of model compounds in artificial sebum. Int J Pharm 345:88-94.

33. Valiveti S, Wesley J, Lu GW 2008. Investigation of drug partition property in artificial sebum. Int J Pharm 346:10-16.

34. Morrison GC, Weschler CJ, Beko G 2016. Dermal uptake directly from air under transient conditions: advances in modeling and comparisons with experimental results for human subjects. Indoor Air 2016:12277.

35. Mohd F, Todo H, Yoshimoto M, Yusuf E, Sugibayashi K 2016. Contribution of the hair follicular pathway to total skin permeation of topically applied and exposed chemicals. Pharmaceutics 8:32-44.

36. Khyat AE, Mavon A, Leduc M, Agache P, Humbert P 1996. Skin critical surface tension: a way to assess the skin wettability quantitatively. Skin Res Technol 2:91-96.

37. Mavon A, Zahouani H, Redoules D, Agache P, Gall Y, Humbert P 1997. Sebum and human surface lipids increase skin surface free energy as measured by contact angle measurements: A study on two anatomical sites. Coll Surf B 8:147-155.

38. Kasting GB, Miller MA 2006. Kinetics of finite dose absorption through skin 2. Volatile compounds. J Pharm Sci 95:268-280.

39. Miller MA, Kasting GB 2015. A spreadsheet-based method for simultaneously estimating the disposition of multiple ingredients applied to skin. J Pharm Sci 104:2047-2055.

40. Haftka JJH, Parsons JR, Govers HAJ 2006. Supercooled liquid vapour pressures and related thermodynamic properties of polycyclic aromatic hydrocarbons determined by gas chromatography. J Chrom A 1135:91-100.

41. Jaworska J, Yu F, Sealschott S, Kasting GB 2021. Thermodynamic properties of nicotinamide/water solutions and their impact on nicotinamide membrane permeability. Unpublished data.

42. National Institutes of Health. 2019. PubChem. Available at : https://pubchem.ncbi.nlm.nih.gov/ Accessed 5/1/2021.

43. Charman WN, Lai CSC, Finnin BC, Reed BL 1991. Self-association of nicotinamide in aqueous solution: mass transport, freezing-point depression, and partition coefficient studies. Pharm Res 8:1144-1150.

44. Coffman RE, Kildsig DO 1996. Self-association of nicotinamide in aqueous solution: light scattering and vapor pressure osmometry studies. J Pharm Sci 85:848-853.

45. Kasting GB, Barai ND 2003. Equilibrium water sorption in human stratum corneum. J Pharm Sci 92:1624-1631.

46. Hansen S, Selzer D, Schaefer UF, Kasting GB 2011. An extended database of keratin binding. J Pharm Sci 100:1712-1726.

47. Harding CR 2004. The stratum corneum: structure and function in health and disease Dermatol Ther 17 Suppl. 1:6-15.

48. Anissimov YG, Roberts MS 2004. Diffusion modeling of percutaneous absorption kinetics: 3. Variable diffusion and partition coefficients, consequences for stratum corneum depth profiles and desorption kinetics. J Pharm Sci 93:470-487.

49. Potts RO, Guy RH 1992. Predicting skin permeability. Pharm Res 9:663-669.

50. Kasting GB, Miller MM, Talreja PS. 2005. Evaluation of stratum corneum heterogeneity. In Bronaugh RL, Maibach HI, eds. Percutaneous Absorption, 4th ed., New York: Taylor & Francis. pp 193-212.

51. Dal Pozzo A, Donzelli G, Liggeri E, Rodriguez L 1991. Percutaneous absorption of nicotinic acid derivatives in vitro. J Pharm Sci 80:54-57.

52. Degim IT, Pugh WJ, Hadgraft J 1998. Skin permeability data: anomalous results. Int J Pharm 170:129-133.

53. Kasting GB, Filloon TG, Francis WR, Meredith MP 1994. Improving the sensitivity of in vitro skin penetration experiments. Pharm Res 11:1747-1754.

54. Akomeah F, Martin G, Brown M 2007. Variability in human skin permeability in vitro: comparing penetrants with different physicochemical properties. J Pharm Sci 96:824-834.

55. Nitsche JM, Wang T-F, Kasting GB 2006. A two-phase analysis of solute partitioning into the stratum corneum. J Pharm Sci 95:649-666.

56. Gajjar RM, Miller MA, Kasting GB 2013. Evaporation of volatile organic compounds from human skin in vitro. Ann Occup Hyg 57:853-865.

57. Chen L, Lian G, Han L 2010. Modeling transdermal permeation. Part I. Predicting skin permeability of both hydrophobic and hydrophilic solutes. AIChE J 56:1136-1146.

58. Chen L, Han L, Lian G 2013. Recent advances in predicting skin permeability of hydrophilic solutes. Adv Drug Deliv Revs 65:295–305.

59. Blume-Peytavi U, Massoudy L, Patzelt A, Lademann J, Dietz E, Rasulev U, Bartels NG 2010. Follicular and percutaneous penetration pathways of topically applied minoxidil foam. Eur J Pharm Biopharm 76:450-453.

60. Frasch H, Barbero A, Hettick J, Nitsche J 2011. Tissue binding affects the kinetics of theophylline diffusion through the stratum corneum barrier layer of skin. J Pharm Sci 100:2989–2995.

61. Seif S, Hansen S 2012. Measuring the stratum corneum reservoir: desorption kinetics from keratin. J Pharm Sci 101:3718-3728.

62. Simulations Plus 2021. TCAT module for GastroPlus. Simulations Plus, Inc., Lancaster, CA USA. Description available at https://www.simulations-plus.com/software/gastroplus/additional-dosage/.

63. Certara 2021. Simcyp PBPK, Certara, Inc., Princeton, NJ USA. Description vailable at https://www.certara.com/company/contact/?referer=https://www.certara.com/software/simcyp-pbpk/.

64. Schwobel JAH, Klamt A 2019. Mechanistic skin penetration model by the COSMOperm method: Routes of permeation, vehicle effects and skin variations in the healthy and compromised skin. Computational Toxicol 11:50-64.

65. Moore TC, Iacovella CR, Leonhard AC, Bunge AL, McCabe C 2018. Molecular dynamics simulations of stratum corneum lipid mixtures: A multiscale perspective. Biochem Biophys Res Commun 498:313-318.

66. Schwobel JAH, Ebert A, Bitterman K, Huniar U, Goss K-U, Klamt A 2020. COSMOperm: mechanistic prediction of passive membrane permeability for neutral compounds and ions and Its pH dependence. J Phys Chem B 124:3343-3354.

67. Fedorowicz A, Milller MA, Frasch HF, Kasting GB. 2011. Finite dose skin permeation calculator. NIOSH. Available at http://www.cdc.gov/niosh/topics/skin/finiteSkinPermCalc.html.

68. Open Systems Pharmacology 2021. Skin permeation model. Avalailable at https://github.com/Open-Systems-Pharmacology/Skin-permeation-model. Accessed July 5, 2021.

69. Ostrenga JA, Steinmetz C, Poulsen BJ 1971. The significance of vehicle composition I. Relationship between topical vehicles composition, skin penetrability and clinical efficacy. J Pharm Sci 60:1175-1179.